Letters

A High Misalignment Tolerance SCC-WPT System With Relay Single Capacitive Coupler for UAV Wireless Charging Applications

Xingchu Lv, Xin Dai, *Member, IEEE*, Fengye Yu, Xiaofei Li, *Member, IEEE*, Heshou Wang, Yue Sun, and Jiefeng Hu, *Senior Member, IEEE*

***Abstract*—This letter proposes a single capacitive coupled wireless power transfer (SCC-WPT) system for unmanned aerial vehicle (UAV) wireless charging applications. By using the inherent UAV helipad as the relay plate, a constant voltage output is achieved. Furthermore, the SCC-WPT system circuits are well presented and analyzed in this letter, and strong misalignment tolerance performance in horizontal as well as rotational situations can be effectively achieved. An experimental prototype was developed, and the experimental results verify that the system can not only maintain stable output voltage under extremely strong misalignment conditions (when the receiver of the system is placed at any position in the *xOy* plane on the relay plate or rotates 360°) but also achieve constant output voltage when the load changes. The experimental results greatly agree with the theoretical analysis.**

***Index Terms*—Capacitive power transfer (CPT), strong misalignment tolerance, unmanned aerial vehicles (UAVs), wireless power transfer (WPT).**

I. Introduction

UNMANNED aerial vehicles (UAVs) are capable of executing tasks, such as reconnaissance, rescue, agricultural management, logistics, and transportation [1], [2]. The escalating demand for their endurance and operational versatility is propelled by their extensive application range. Nowadays, there emerges a necessity for automatic wireless charging capabilities that can offer uninterrupted power support for UAVs during field missions, thereby augmenting their flexibility and adaptability.

Within the realm of wireless power transfer technology, the conventional UAV-related wireless charging systems mainly focused on inductive power transfer (IPT) technology. For example, researchers have proposed a constant current output control method for multiple-drone in-flight wireless charging systems with air-core coils [3], with the objective of improving the stability and reliability of UAV hovering wireless charging. However, drone wireless charging systems using air-core coils have high electromagnetic interference (EMI), which can cause interference with sensitive electronic equipment in the drone [4]. To overcome the EMI problems caused by the air-core coil, Song et al. [5] added ferrite to the coil; thereby, the EMI outside the coupling mechanism is greatly reduced. Unfortunately, adding ferrite will increase the weight of the power receiver of the system, thereby decreasing the cruising range of the drone [6].

Given the limitations inherent in applying IPT-based UAV wireless charging systems, capacitive power transfer (CPT) technology has emerged as a viable alternative by utilizing lightweight conductive plates, thereby obviating the need for heavy litz wire and ferrite. Mostafa et al. [7] proposed a CPT-based drone wireless charging system, which achieves the lightweight of the power receiver and overcomes EMI issues to a certain extent. However, the system's misalignment tolerance is relatively poor since the CPT system has four plates; once any pair of plates is misaligned, the energy efficiency characteristics of the system will be reduced. Another CPT scheme proposed in [8] possesses lateral misalignment tolerance but weak longitudinal antioffset performance. In recent years, Liu et al. [9] have proposed a single capacitive coupled wireless power transfer (SCC-WPT) system to achieve a lightweight coupling mechanism. In addition, the system has strong misalignment tolerance. Hence, this technology in UAV wireless charging applications can be further studied.

In light of the challenges previously delineated, this letter proposes an SCC-WPT system for UAV wireless charging applications. By using a UAV helipad as a relay plate, this system can overcome space constraints and weight issues and achieve the requirement of high misalignment tolerance.

The main innovative contributions of this letter can be summarized as follows.

1) This letter proposes an SCC-WPT system for UAV wireless charging applications. Compared to the IPT-based wireless charging methods shown in [4] and [5], the weight is comparable.

Received 5 December 2024; revised 25 January 2025 and 2 March 2025; accepted 21 March 2025. Date of publication 25 March 2025; date of current version 26 May 2025. This work was supported by the National Natural Science Foundation of China under Grant 52277003. *(Corresponding authors: Xiaofei Li; Heshou Wang.)*

Xingchu Lv, Xin Dai, Fengye Yu, Xiaofei Li, and Yue Sun are with the School of Automation, Chongqing University, Chongqing 400044, China (e-mail: 20221301023@stu.cqu.edu.cn; daixin@cqu.edu.cn; 202313021020@stu.cqu.edu.cn; xiaofei.li@cqu.edu.cn; syue06@cqu.edu.cn).

Heshou Wang is with the Department of Electrical Engineering, The Hong Kong Polytechnic University, Hung Hom 999077, Hong Kong (e-mail: hs.wang@polyu.edu.hk).

Jiefeng Hu is with the Centre for New Energy Transition Research, Federation University Australia, Mount Helen, VIC 3353, Australia (e-mail: j.hu@federation.edu.au).

Color versions of one or more figures in this article are available at https://doi.org/10.1109/TPEL.2025.3554676.

Digital Object Identifier 10.1109/TPEL.2025.3554676

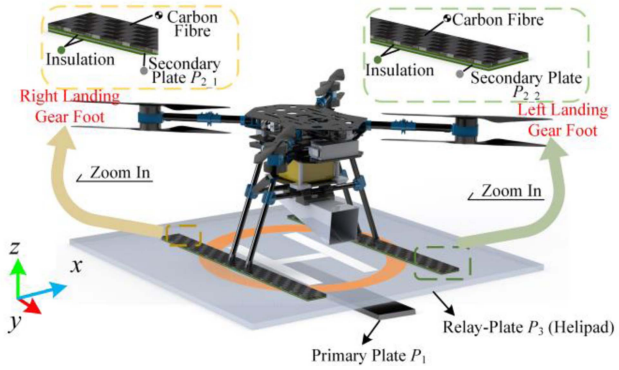

Fig. 1. Overview of the proposed SCC-CPT system.

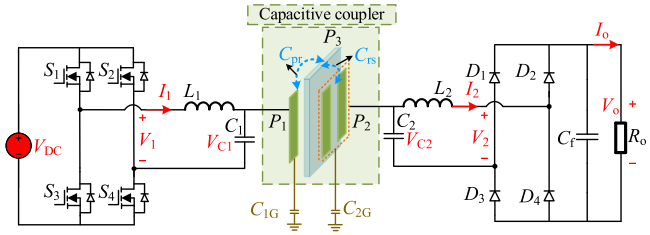

Fig. 2. Circuit topology of the proposed SCC-CPT system.

2) This letter leverages the advantages of the SCC-WPT system, enabling the system to achieve constant voltage (CV) output under extremely misaligned conditions without additional control circuits. This letter can achieve CV output under 360° rotation, while paper [8] can only achieve it under 45° rotation. This letter can achieve CV output without additional control circuits, when the receiver of the system is placed at any position in the *xOy* plane on the relay plate, while paper [10] can only achieve it under a single axial offset. As for [11], the transmitter plates need to be controlled based on the position of the receiver.

II. Proposed System With High Misalignment Tolerance Performance

A. System Overview

Fig. 1 illustrates the proposed UAV wireless charging system, and both drone landing gears have been modified with metal plates installed at the bottom, referred to as P_{2_1} and P_{2_2}, respectively. They are connected in series to form P_2 in the circuit shown in Fig. 2, functioning as a receiver. This allows for the balance between the left- and right-hand sides. This configuration enhances the coupling capability while without wasting space on UAVs. In addition to secondary plate P_2 elucidated in Fig. 1, the capacitive coupler proposed in this letter includes a primary plate P_1 and a drone helipad as a relay plate P_3.

B. Circuit Analysis

The circuit topology of the proposed SCC-CPT system is shown in Fig. 2, where plates P_1 and P_2, in conjunction with the relay plate P_3, function collectively as a capacitive coupler.

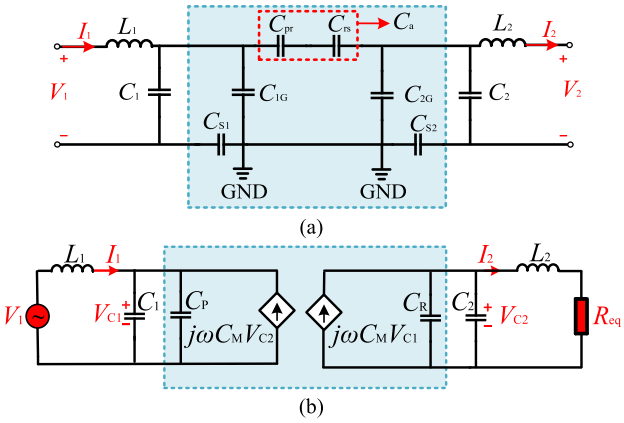

Fig. 3. Equivalent circuit of the proposed SCC-WPT system. (a) Model of the circuit with the stray capacitance and self-capacitance. (b) Behavior-source model.

The input dc voltage of the system is V_{DC}. L_1 and C_1 are the compensating inductor and capacitor on the primary side, respectively, while L_2 and C_2 are the compensating inductor and capacitor on the secondary side, respectively. C_f and R_o are the filtering capacitor and the load resistance, respectively. The conversion in the H-bridge inverter and the full-bridge rectifier can be expressed as $V_1 = 2\sqrt{2}V_{DC}/\pi$ and $R_{eq} = R_o \times 8/\pi^2$, respectively.

Fig. 3(a) illustrates the equivalent circuit model of the system when considering the stray capacitance, where mutual capacitances C_{pr} and C_{rs} are formed between (P_1, P_3) and (P_2, P_3), respectively. In Fig. 3(a), stray capacitances C_{S1} and C_{S2} between the circuit and the earth ground provide the current-returning paths for the primary and secondary circuits, respectively [12], [13]. Moreover, according to Minteer [14], C_{1G} and C_{2G} are formed by two metal plates P_1 and P_2 in free space, which can be calculated as

$$C_{1G} = C_{2G} = 4\varepsilon_0\sqrt{\frac{S}{\pi}} \tag{1}$$

where S represents the area of the rectangular plate.

Furthermore, such a circuit can be represented by an equivalent behavior-source model [13], as shown in Fig. 3(b), where C_M is defined as the mutual capacitance, while C_P and C_R are defined as the self-capacitances. In the proposed system, C_P, C_R, and C_M can be derived as

$$\begin{cases} C_M = \frac{C_{s1}C_{s2}C_a}{(C_{1G}+C_{s1}+C_a)(C_{2G}+C_{s2}+C_a)-C_a^2} \\ C_P = C_{s1} - \frac{C_{s1}^2(C_{2G}+C_{s2}+C_a)}{(C_{1G}+C_{s1}+C_a)(C_{2G}+C_{s2}+C_a)-C_a^2} - C_M \\ C_R = C_{s2} - \frac{C_{s2}^2(C_{1G}+C_{s1}+C_a)}{(C_{1G}+C_{s1}+C_a)(C_{2G}+C_{s2}+C_a)-C_a^2} - C_M \end{cases} \tag{2}$$

where C_a is the series value of C_{pr} and C_{rs}, which can be calculated as

$$C_a = \frac{1}{\frac{1}{C_{pr}} + \frac{1}{C_{rs}}}. \tag{3}$$

In order to achieve an identical resonant network and simplify calculations, it is assumed that

$$\begin{cases} C_1 = C_2 \\ L_1 = L_2. \end{cases} \tag{4}$$

According to Kirchhoff's Voltage Law and Kirchhoff's Current Law, the following equations can be obtained:

$$\begin{cases} V_1 = j\omega L I_1 + V_{C_1} \\ V_2 = V_{C_2} - j\omega L I_2 = I_2 R_{\text{eq}} \\ I_1 + j\omega(C_1 + C_P)V_{C_1} = j\omega C_M V_{C_2} \\ I_2 + j\omega(C_2 + C_R)V_{C_2} = j\omega C_M V_{C_1}. \end{cases} \tag{5}$$

By solving (5), the output voltage V_2 can be calculated as

$$V_2 = -V_1 + j \left(\frac{L^2\omega^3(C_1 + C_P)V_1}{R_{\text{eq}}} - \frac{L^2\omega^3 C_M V_1}{R_{\text{eq}}} - \frac{V_1 \omega L}{R_{\text{eq}}} \right). \tag{6}$$

It can be seen from (6) that the secondary ac voltage V_2 is independent of the load.

To achieve a load-independent CV output, the operating frequency of the system can be derived as

$$\omega_{\text{CV}} = \sqrt{\frac{1}{(C_1 + C_P - C_M)L}}. \tag{7}$$

As seen in (2) and (7), the working frequency changes with the variation of $C_{1\text{G}}$ and $C_{2\text{G}}$. According to (6), (7), and $V_1 = 2\sqrt{2}V_{\text{DC}}/\pi$, the output dc voltage V_o can be represented as

$$V_o = V_{\text{DC}}. \tag{8}$$

Furthermore, by solving (5), the input impedance Z_{in} can be obtained as

$$Z_{\text{in}} = \frac{V_1}{I_1} = \frac{R_{\text{eq}}}{1 + \left(-\frac{R_{\text{eq}}(C_1 + C_P)}{C_M \omega L} - \frac{R_{\text{eq}}}{\omega L} \right)^2} + j \frac{R_{\text{eq}} \left(\frac{R_{\text{eq}}(C_1 + C_P)}{C_M \omega L} + \frac{R_{\text{eq}}}{\omega L 1} \right)}{1 + \left(-\frac{R_{\text{eq}}(C_1 + C_P)}{C_M \omega L} - \frac{R_{\text{eq}}}{\omega L} \right)^2}. \tag{9}$$

In (9), it can be derived that its imaginary part is always greater than 0, so the system can maintain zero-voltage switching (ZVS).

C. Misalignment Tolerance Performance Analysis

As shown in Fig. 4(a) and (b), the length l of both P_1 and P_2 is 400 mm. The width of P_1 is 100 mm. The width of both P_{2_1} and P_{2_2} is 50 mm. The overlapping areas between parallel plates P_1 and P_3 are denoted as A_1. Similarly, the overlapping area between P_2 and P_3 is represented by A_2. Therefore, as long as P_1 and P_2 are within the coverage of P_3, $A_1 = A_2$. The distance between P_1 and P_3 (P_2 and P_3) is defined as d_1 (d_2), where $d_1 = d_2 = 3$ mm. The length and width of P_3 are 450 mm each, and the thickness is 15 mm.

When the drone lands on the charging platform (i.e., the helipad), lateral misalignment (x-axis displacement), longitudinal misalignment (y-axis displacement), or angular misalignment will occur. Therefore, analyzing the misalignment tolerance performance of the free landing coupling mechanism proposed in this letter is crucial. Fig. 4 shows that lateral, longitudinal, and angular offset misalignment occurs to P_2, and P_1 and P_3 are fixed. In Fig. 4(a), the centers of P_1 and P_2 coincide, while Fig. 4(b) illustrates arbitrary misalignment of the centers of P_2 on the xOy plane, with a range of Δx from –75 to 75 mm and Δy from –25 to 25 mm, where Δx and Δy represent the relative misalignments of the center between P_1 and P_2 on the x- and y-axes, respectively. In Fig. 4(c), the P_2 plate undergoes arbitrary angle rotation on the xOy plane, where "α" represents the rotation angle of P_2.

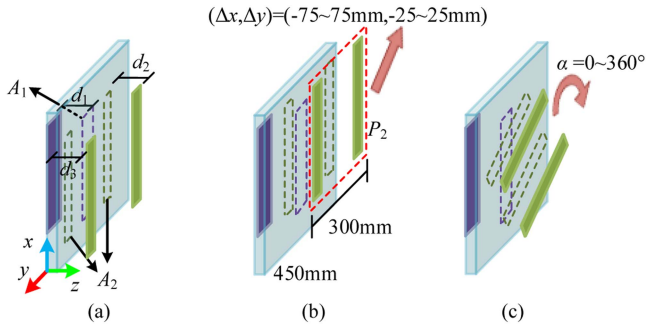

Fig. 4. Lateral, longitudinal, and angular offset misalignment occurs between P_1, P_2, and P_3. (a) Center alignment. (b) Lateral and longitudinal misalignment. (c) Rotation angle from 0° to 360°.

TABLE I
SYSTEM PARAMETERS

Parameter	Value	Parameter	Value	Parameter	Value
V_{DC}	44V	C_{pr}	116 pF	C_{rs}	116.2 pF
C_1	100.2 pF	C_{S1}	3.1 pF	R_o	30 Ω
C_2	100.4 pF	C_{S2}	3.3 pF	f	1.5 MHz
L_1	112.3 μH	L_2	111.8 μH		

As for mutual capacitances C_{pr} and C_{rs}, the value can be calculated as [14]

$$C = \frac{\varepsilon_0 \varepsilon_r A}{d} \tag{10}$$

where ε_0 is the electric constant $\varepsilon_0 \approx 8.854 \times 10^{-12}\text{F}\cdot\text{m}^{-1}$, ε_r is the dielectric constant of the dielectric material filled between plates, d is the separation between the plates, and A is the coupling area. It can be seen that ε_0, ε_r, and d are all fixed. As long as A remains unchanged, the mutual capacitance values C_{pr} and C_{rs} will also remain unchanged.

Consequently, in the event of x- and y-axis misalignment between P_1 and P_2, as long as A_1 and A_2 remain unchanged, the capacitance constructed of two parallel plates will also be fixed. That is because the mutual capacitances C_{pr} and C_{rs} in (3) remain stable, which means that C_M in (2) and (7) remains unchanged. It can be seen from (7) that only when the system operates at this frequency can the secondary ac voltage V_2 in (6) remain unchanged, thereby achieving CV output.

III. EXPERIMENTAL RESULTS

An experimental prototype is constructed, as depicted in Fig. 5. The system parameters can be found in Table I.

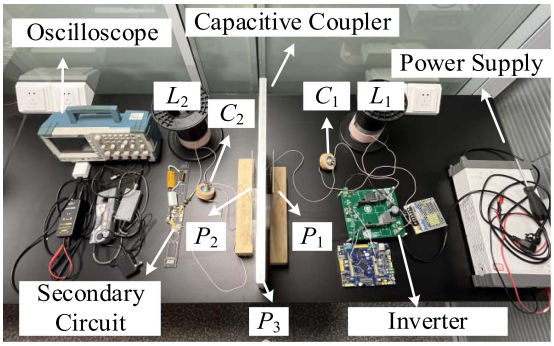

Fig. 5. Photographs of the experimental setup.

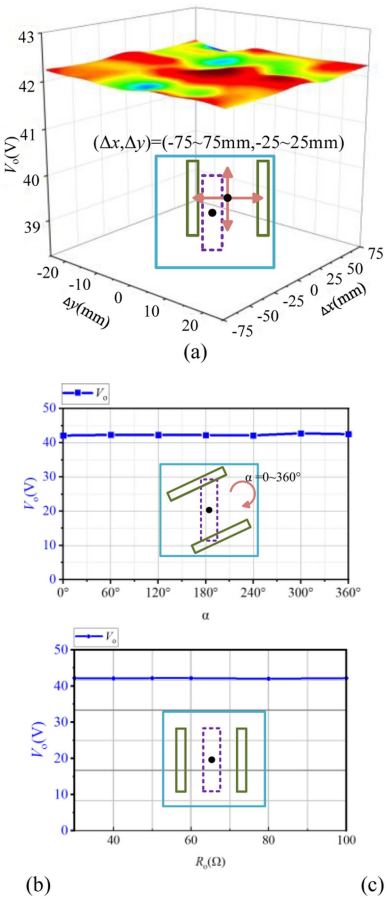

Fig. 6. Variation of the output DC voltage. (a) Δx from –75 to 75 mm and Δy from –25 to 25 mm. (b) Rotation of 360° of the secondary plate. (c) Output DC voltage V_o as the load resistance R_o changes.

Fig. 6(a) illustrates the fluctuations in system output voltage in response to Δx from –75 to 75 mm and Δy from –25 to 25 mm, which shows that the output voltage consistently maintains 42.2 V $\pm$ 0.83%, verifying the stability of the response to the xOy plane misalignment. Meanwhile, the experimental result of arbitrary angle rotation of P_2 in the xOy plane is presented in Fig. 6(b), which shows that the output voltage consistently maintains 42.2 V $\pm$ 0.45%, verifying the stability of the response to the angle rotation misalignment. These results suggest that the output voltage remains fundamentally stable, thereby

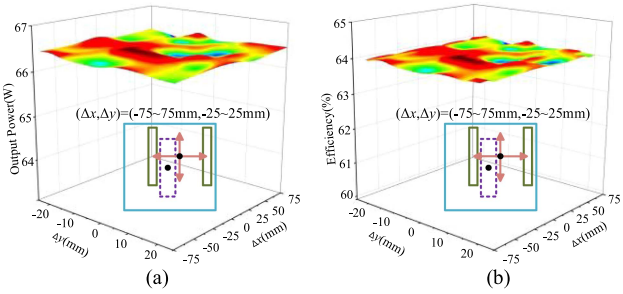

Fig. 7. Output power and efficiency results. (a) Output power with Δx from –75 to 75 mm and Δy from –25 to 25 mm. (b) Efficiency with Δx from –75 to 75 mm and Δy from –25 to 25 mm.

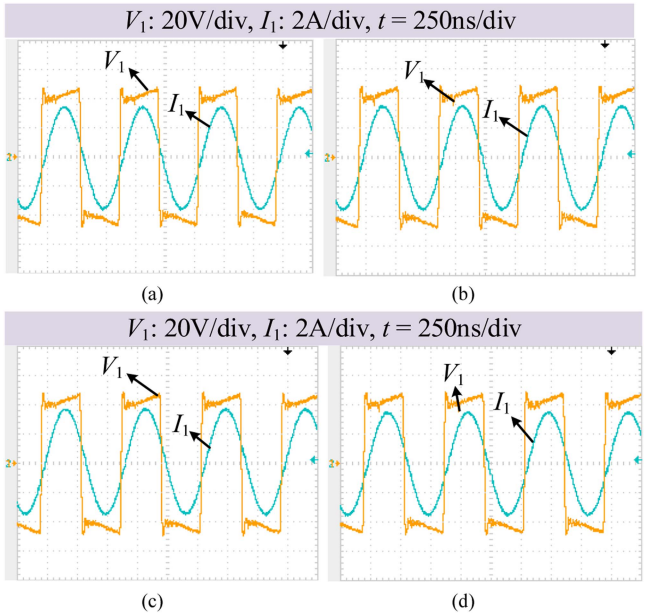

Fig. 8. Experimental waveforms of V_1 and I_1. (a) Center alignment. (b) Δx = 75 mm and Δy = 25 mm. (c) Rotation of 30° of the secondary plate (R_o = 30 Ω). (d) Rotation of 30° of the secondary plate (R_o = 35 Ω).

corroborating the effectiveness of the high-misalignment tolerance in the presented system. In addition, Fig. 6(c) shows the variation curves of the system output dc voltage V_o as the load resistance R_o changes from 30 to 100 Ω, while the output dc voltage is generally sustained at 42.2 V $\pm$ 0.5%. These results suggest that the system possesses CV output characteristics.

Fig. 7(a) and (b) illustrates the fluctuations in system output power and efficiency in response to Δx from –75 to 75 mm and Δy from –25 to 25 mm. The output power fluctuates around 66.4 W, while the efficiency fluctuates around 64.1%.

Fig. 8 shows the output voltage and current of the inverter, with center alignment [see Fig. 8(a)], Δx = 75 mm and Δy = 25 mm [see Fig. 8(b)], and rotation of 30° of P_2 [see Fig. 8(c)]. It can be discerned that the input voltage and current, i.e., V_1 and I_1, in these three cases remain nearly unchanged, and the inverter keeps working in an ideal ZVS state. This indicates that the resonant parameters are unaltered due to the consistent capacitance among P_1, P_2, and P_3 according to (10) under different misalignment conditions. In addition to Fig. 8(c), which

TABLE II
COMPARISONS OF DIFFERENT SYSTEMS FOR UAVS

Reference	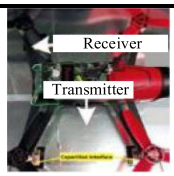 [8]	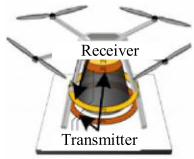 [10]	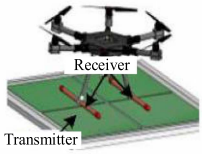 [11]	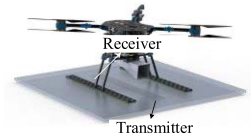 This letter
Number of coupled plate pairs	Two	Two	Two	One
Receiver installation difficulty	★★★	★★★	★	★
Control difficulty	★★	★	★★★	★
Lateral misalignment(Δx)	Δx =(−20 mm,20 mm)	/	Δx =(−100 mm,100 mm)	Δx=(−75 mm ,75 mm),
Longitudinal misalignment(Δy)	/	/	Δy =(−100 mm,100 mm)	Δy =(−25 mm ,25 mm)
Rotational misalignment	−45°−45°	0–360°	0–360°	0–360°

"★" means the degree of difficulty. The more "★" there is, the worse the performance. "/" means that lateral misalignment issues cannot be overcome.

shows the output voltage and current of the inverter when R_o = 30 Ω, Fig. 8(d) shows the case of R_o = 35 Ω. By comparing Fig. 8(c) and (d), it can be found that the inverter can still maintain the ZVS state when the load changes.

IV. DISCUSSION

A. Comparison With Other CPT UAV Systems

Table II presents a comparative analysis of different UAV WPT systems, highlighting their number of coupled plate pairs, receiver installation difficulty, control difficulty, and misalignment tolerance. The magnetic coupler proposed in this letter uses one pair of coupled plates, while [8], [10], and [11] all use two pairs of coupled plates. The receiver installation difficulty of this letter is comparable to that of [11], but simpler than that of [8] and [10]. In terms of control difficulty, this letter and [10] do not require additional control circuits, which is simpler than [8] and [11] that require additional control circuits. The method proposed in [8] is limited in adapting to rotational misalignment, while the capacitive couplers proposed in this study and [10] and [11] have an advantage by supporting a 0–360° rotational misalignment. In terms of absolute lateral and longitudinal misalignment range, the misalignment range of this letter and [11] is better than that of [8] and [10]. Although the absolute lateral and longitudinal misalignment range of [11] is larger than that of this letter, the misalignment tolerance performance of this letter is comparable to that of [11], because as long as the receiver lands within the range of the charging platform, constant output can be achieved without additional control circuits.

B. Comparison With Other SCC-WPT Systems

In terms of output power and efficiency of the SCC-WPT system, the comparison results between this letter and [9], [15], and [16] are summarized in Table III. As can be seen from Table III, the efficiency of this letter is higher than that of [9], [15], and [16]. The output power of this letter is suitable for DJI Matrice 350 RTK UAV; it is higher than that of [15] and [16], but lower than that of [9].

TABLE III
COMPARISONS OF DIFFERENT SCC-WPT SYSTEMS

Reference	Efficiency	Output power
[9]	62%	266 W
[15]	53.4%	20 W
[16]	35%	3.6 W
This letter	64.1%	66.4 W

V. CONCLUSION

This letter presents an SCC-CPT system characterized by strong misalignment tolerance performance; this system can maintain an output voltage of 42.2 V ± 0.83% when the secondary plate P_2 of the coupling mechanism is strongly misaligned from (Δx, Δy) = (–75 mm, –25 mm) to (Δx, Δy) = (75 mm, 25 mm). Equally impressive is that this system can maintain an output voltage of 42.2 V ± 0.45% when the secondary plate P_2 rotation angle of the coupling mechanism changes from 0° to 360°. Meanwhile, this system achieves an output voltage of 42.2 V ± 0.5% when the load changes within the range of 30–100 Ω. The inverter of this system keeps working in an ideal ZVS state when the receiver of the system is placed at any position in the xOy plane on the relay plate or rotates 360° and when the load changes. The SCC-WPT system proposed in this letter has a total weight of 60.5 g for the secondary plate and secondary circuit, which is applied to DJI Matrice 350 RTK. It is estimated that with the addition of this system, the flight duration of the drone will be reduced from the original 44.9 to 44.5 min. In addition, the impact of the environment on the parameters of this system will be further studied in the future work.

REFERENCES

[1] H. Shakhatreh et al., "Unmanned aerial vehicles (UAVs): A survey on civil applications and key research challenges," *IEEE Access*, vol. 7, pp. 48572–48634, 2019.

[2] J. Kim, S. Kim, C. Ju, and H. I. Son, "Unmanned aerial vehicles in agriculture: A review of perspective of platform, control, and applications," *IEEE Access*, vol. 7, pp. 105100–105115, 2019.

[3] Y. Gong, Z. Zhang, and S. Chang, "Single-transmitter-controlled multiple-channel constant current outputs for in-flight wireless charging of drones," *IEEE Trans. Ind. Electron.*, vol. 71, no. 4, pp. 3606–3616, Apr. 2024.

[4] J. Zhou, B. Zhang, W. Xiao, D. Qiu, and Y. Chen, "Nonlinear parity-time-symmetric model for constant efficiency wireless power transfer: Application to a drone-in-flight wireless charging platform," *IEEE Trans. Ind. Electron.*, vol. 66, no. 5, pp. 4097–4107, May 2019.

[5] C. Song et al., "EMI reduction methods in wireless power transfer system for drone electrical charger using tightly coupled three-phase resonant magnetic field," *IEEE Trans. Ind. Electron.*, vol. 65, no. 9, pp. 6839–6849, Sep. 2018.

[6] Y. Chang, X. Zhang, C. Ma, W. Huang, and H. Yan, "A constant voltage/current CPT system with lightweight characteristics for the unmanned aerial vehicle," *IEEE Access*, vol. 12, pp. 1737–1746, 2024.

[7] T. M. Mostafa, A. Muharam, and R. Hattori, "Wireless battery charging system for drones via capacitive power transfer," in *Proc. IEEE PELS Workshop Emerg. Technol.: Wirel. Power Transfer*, 2017, pp. 1–6.

[8] A. Muharam, T. M. Mostafa, and R. Hattori, "Design of power receiving side in wireless charging system for UAV application," in *Proc. Int. Conf. Sustain. Energy Eng. Appl.*, 2017, pp. 133–139.

[9] Z. Liu, Y. Su, H. Hu, Z. Deng, and R. Deng, "Research on transfer mechanism and power improvement technology of the SCC-WPT system," *IEEE Trans. Power Electron.*, vol. 38, no. 1, pp. 1324–1335, Jan. 2023.

[10] C. Park et al., "Separated circular capacitive coupler for reducing cross-coupling capacitance in drone wireless power transfer system," *IEEE Trans. Microw. Theory Techn.*, vol. 68, no. 9, pp. 3978–3985, Sep. 2020.

[11] C. Cai, X. Liu, S. Wu, X. Chen, W. Chai, and S. Yang, "A misalignment tolerance and lightweight wireless charging system via reconfigurable capacitive coupling for unmanned aerial vehicle applications," *IEEE Trans. Power Electron.*, vol. 38, no. 1, pp. 22–26, Jan. 2023.

[12] H. Zhang, F. Lu, H. Hofmann, W. Liu, and C. C. Mi, "A four-plate compact capacitive coupler design and LCL-compensated topology for capacitive power transfer in electric vehicle charging application," *IEEE Trans. Power Electron.*, vol. 31, no. 12, pp. 8541–8551, Dec. 2016.

[13] F. Lu, H. Zhang, and C. Mi, "A two-plate capacitive wireless power transfer system for electric vehicle charging applications," *IEEE Trans. Power Electron.*, vol. 33, no. 2, pp. 964–969, Feb. 2018.

[14] T. M. Minteer, "The many capacitance terms of two parallel discs in free space," *Eur. J. Phys.*, vol. 35, no. 3, pp. 99–106, 2014.

[15] X. Gao, H. Zhou, W. Hu, Q. Deng, G.-P. Liu, and J. Lai, "Capacitive power transfer through virtual self-capacitance route," *Int. Eng. Technol. Power Electron.*, vol. 11, no. 6, pp. 1110–1118, 2018.

[16] L. J. Zou, Q. Zhu, C. W. Van Neste, and A. P. Hu, "Modeling single wire capacitive power transfer system with strong coupling to ground," *IEEE J. Emerg. Sel. Top. Power Electron.*, vol. 9, no. 2, pp. 2295–2302, Apr. 2021.